nature chemical biology

ARTICLES

https://doi.org/10.1038/s41589-020-0484-2

Check for updates

A drug discovery platform to identify compounds that inhibit EGFR triple mutants

Punit Saraon[1,23], Jamie Snider[1,23], Yannis Kalaidzidis[2], Leanne E. Wybenga-Groot[3], Konstantin Weiss[1], Ankit Rai[4], Nikolina Radulovich[5], Luka Drecun[1,6], Nika Vučković[1], Adriana Vučetić[1], Victoria Wong[1], Brigitte Thériault[7], Nhu-An Pham[5], Jin H. Park[8,22], Alessandro Datti[9,10], Jenny Wang[9], Shivanthy Pathmanathan[1,6], Farzaneh Aboualizadeh[1], Anna Lyakisheva[1], Zhong Yao[1], Yuhui Wang[5], Babu Joseph[7], Ahmed Aman[7], Michael F. Moran[11,12], Michael Prakesch[7], Gennady Poda[7,13], Richard Marcellus[7], David Uehling[7], Miroslav Samaržija[14], Marko Jakopović[14], Ming-Sound Tsao[5,15,16], Frances A. Shepherd[17,18], Adrian Sacher[5], Natasha Leighl[5], Anna Akhmanova[4], Rima Al-awar[7,19], Marino Zerial[2] and Igor Stagljar[1,6,20,21] ✉

Receptor tyrosine kinases (RTKs) are transmembrane receptors of great clinical interest due to their role in disease. Historically, therapeutics targeting RTKs have been identified using in vitro kinase assays. Due to frequent development of drug resistance, however, there is a need to identify more diverse compounds that inhibit mutated but not wild-type RTKs. Here, we describe MaMTH-DS (mammalian membrane two-hybrid drug screening), a live-cell platform for high-throughput identification of small molecules targeting functional protein–protein interactions of RTKs. We applied MaMTH-DS to an oncogenic epidermal growth factor receptor (EGFR) mutant resistant to the latest generation of clinically approved tyrosine kinase inhibitors (TKIs). We identified four mutant-specific compounds, including two that would not have been detected by conventional in vitro kinase assays. One of these targets mutant EGFR via a new mechanism of action, distinct from classical TKI inhibition. Our results demonstrate how MaMTH-DS is a powerful complement to traditional drug screening approaches.

RTKs are an important class of integral membrane cell surface receptors, responsible for triggering diverse intracellular signaling cascades in response to external stimuli and playing a chief role in regulating many cellular processes[1]. They all share a similar tripartite architecture, with an extracellular, ligand-binding region, a single alpha-helical membrane spanning domain and a cytoplasmic region containing a tyrosine kinase domain alongside C-terminal and juxtamembrane regulatory elements[1,2]. Binding of ligand to RTK monomers induces dimerization and conformational changes, leading to activation of the intracellular tyrosine kinase domains, trans-autophosphorylation of tyrosine residues and recruitment/activation of intracellular signaling proteins. Due to their central importance, RTK dysfunction is causally associated with a variety of diseases (including many cancers) making them targets of therapeutic importance[1].

So far, small molecules targeting RTK activity have been primarily identified using in vitro kinase assays, powerful enzymatic methods suited for high-throughput screening of tens to hundreds of thousands of compounds in parallel. By necessity, these assays are performed outside the natural cellular environment, using purified kinase domain instead of full-length protein, introducing a number of limitations[3]. One notable limitation is the inability to detect compounds that affect RTK function independent of direct inhibition of kinase activity, or whose action depends on additional protein domains or cellular factors, potentially leading to molecules of therapeutic value being missed. Moreover, in vitro kinase assays do not assess cellular toxicity or permeability of molecules, leading to the identification of numerous candidates found to be impractical for use in follow-up testing. Other common assays, such as cell viability approaches, offer the natural environmental advantages of working

[1]Donnelly Centre, University of Toronto, Toronto, Ontario, Canada. [2]Max Planck Institute of Molecular Cell Biology and Genetics, Dresden, Germany. [3]SPARC BioCentre, The Hospital for Sick Children, Toronto, Ontario, Canada. [4]Cell Biology, Department of Biology, Faculty of Science, Utrecht University, Utrecht, the Netherlands. [5]Princess Margaret Cancer Centre, University Health Network, University of Toronto, Toronto, Ontario, Canada. [6]Department of Molecular Genetics, University of Toronto, Toronto, Ontario, Canada. [7]Drug Discovery Program, Ontario Institute for Cancer Research, Toronto, Ontario, Canada. [8]Department of Pharmacology and Cancer Biology Institute, Yale University, New Haven, CT, USA. [9]Network Biology Collaborative Centre, Lunenfeld-Tanenbaum Research Institute, Mount Sinai Hospital, Toronto, Ontario, Canada. [10]Department of Agriculture, Food, and Environmental Sciences, University of Perugia, Perugia, Italy. [11]Peter Gilgan Centre for Research and Learning, Hospital for Sick Children, Toronto, Ontario, Canada. [12]Department of Molecular Genetics, University of Toronto, Toronto, Ontario, Canada. [13]Leslie Dan Faculty of Pharmacy, University of Toronto, Toronto, Ontario, Canada. [14]Department for Lung Diseases Jordanovac, Clinical Hospital Centre Zagreb, University of Zagreb, Zagreb, Croatia. [15]Department of Medical Biophysics, University of Toronto, Toronto, Ontario, Canada. [16]Department of Laboratory Medicine and Pathobiology, University of Toronto, Toronto, Ontario, Canada. [17]Division of Medical Oncology and Hematology, Princess Margaret Cancer Centre, University Health Network, Toronto, Ontario, Canada. [18]Department of Medicine, University of Toronto, Toronto, Ontario, Canada. [19]Department of Pharmacology and Toxicology, University of Toronto, Toronto, Ontario, Canada. [20]Department of Biochemistry, University of Toronto, Toronto, Ontario, Canada. [21]Mediterranean Institute for Life Sciences, Split, Croatia. [22]Present address: Department of Pharmacology, Weill Cornell Medicine, New York, NY, USA. [23]These authors contributed equally: Punit Saraon and Jamie Snider. ✉e-mail: igor.stagljar@utoronto.ca

in live cells, but only detect compounds affecting cell growth/metabolism, and do not allow screening using specific disease-associated protein targets, making them less selective.

We previously reported the development of the mammalian membrane two-hybrid (MaMTH)[4], a split-ubiquitin-based technology adapted from our well-established membrane yeast two-hybrid (MYTH)[5–7]. MaMTH is designed to detect protein–protein interactions (PPIs) involving full-length integral membrane proteins directly in their natural membrane context in live mammalian cells[4] (Supplementary Fig. 1). Notably, MaMTH is highly sensitive and able to detect subtle, dynamic alterations in PPIs in response to mutation state and environmental changes[5,8,9].

In this study, we exploit these key features of MaMTH to convert it into a high-throughput, small-molecule screening platform to detect compounds that specifically target RTK functional interactions. This new platform, called MaMTH-DS (for MaMTH drug screening) is highly sensitive, easy to setup up, readily scalable, and combines the specificity of in vitro kinase assays with the advantages of working in live cells. In this way, MaMTH-DS allows identification of compounds inhibiting specific interactions of interest, but with the advantages that this inhibition can be mediated by diverse mechanisms, and that detected compounds are already cell permeable and have their toxicity assessed.

As a proof of principle, we used MaMTH-DS to screen an osimertinib-resistant EGFR mutant important in non-small-cell lung cancer (NSCLC) against a pilot library of 2,960 small molecules and, in conjunction with follow-up assays, identified four mutant-specific compounds. We demonstrate that two of these compounds would not have been identified as specific mutant EGFR-targeting agents by classical in vitro kinase or cell-based assays, and that one of these compounds displays a completely new mechanism of action with respect to its effect on mutant EGFR signaling. Overall, our results illustrate key advantages of MaMTH-DS, including its ability to identify diverse types of compound, and show how it can serve as a powerful complement to traditional drug screening approaches. Additionally, several of the molecules identified in this study are promising candidates for treatment of mutant EGFR-associated, drug-resistant NSCLC for which therapeutic options are currently lacking.

Results

Development of MaMTH-DS platform. To develop MaMTH-DS we introduced several major modifications to traditional MaMTH. The first was a transition from transiently transfected to stably expressed baits, a necessary step to minimize variability/noise and allow for sensitive detection of small-molecule activity in a large-scale multi-well format. To improve ease of stable generation, we made reporter cell lines and MaMTH bait vector compatible with the Flp-IN TREx system (Thermo Fisher), a Flp recombinase-based method for rapid generation of isogenic stables in as little as 2 weeks. Expression of bait in this format is also under the control of a tetracycline-inducible promoter, allowing controlled bait induction during screening. The MaMTH bait vector was also adapted for use with Gateway cloning technology (Thermo Fisher) to facilitate rapid generation of constructs. A schematic diagram of the MaMTH-DS bait vector is given in Supplementary Fig. 2a. Furthermore, to reduce cell loss and make the system compatible with automated handling steps, we greatly enhanced the adherence of our reporter cells to tissue culture plastic by genomic integration and overexpression of the macrophage scavenger receptor (MSR1)[10] (Supplementary Fig. 2b). We also changed our reporter from Firefly to *Gaussia princeps* luciferase, a substantially more stable enzyme that has the advantage of being secreted from cells into the growth media. This eliminates the cell lysis step of the original MaMTH, reducing handling steps and associated variability. Additionally, *G. princeps* luciferase produces significantly higher signal than Firefly luciferase, allowing for more sensitive detection, particularly in a 384-well format (Supplementary Fig. 2c). Collectively these changes make the assay easy to setup, improve sensitivity and signal strength, and greatly reduce variability, permitting its use in an automated, high-throughput, multi-well small-molecule screening system.

Testing and validation of MaMTH-DS. To test MaMTH-DS sensitivity and suitability for use in drug screening, we selected several RTKs whose dysfunction is associated with cancer and prepared stable MaMTH-DS RTK baits in our reporter cell lines. In our assays, we chose Shc1 as a 'prey' since it is well documented to interact with a wide variety of activated RTKs in a spatial-temporal manner and is important for their signaling function[11,12] (although other RTK interactors could also be used). We then performed MaMTH-DS assays in the presence of small-molecule TKIs, including control molecules and compounds known to specifically target the function of the corresponding RTKs. First, we examined the response of the RTK MET to the TKIs crizotinib and erlotinib. As expected, the interaction was strongly reduced in a dose-dependent manner when exposed to crizotinib, consistent with crizotinib's reported activity against MET[13], but not erlotinib, which does not target MET (Supplementary Fig. 3a, left). The response to crizotinib was not due to a loss in cell viability (Supplementary Fig. 3a, middle), although some reduction in bait expression was observed (Supplementary Fig. 3a, right), indicating crizotinib reduces MET stability (and consequently interaction with Shc1). We next tested the response of FGFR4 bait to BLU9931, a compound reported to target this receptor[14]. Similar to our results with MET, reporter activity was strongly reduced in the presence of BLU9931, but not in the presence of erlotinib control (Supplementary Fig. 3b, left). Once again BLU9931 had no effect on reporter cell viability (Supplementary Fig. 3b, middle) but some effect on FGFR4 bait expression was observed (Supplementary Fig. 3b, right), although this was less pronounced than that observed with MET. We then proceeded to examine the response of two additional RTKs, AXL and anaplastic lymphoma kinase (ALK), to the compounds foretinib and brigatinib, previously shown to target these receptors, respectively[15–17]. Once again, AXL and ALK activities were strongly reduced, in a dose-dependent manner, in the presence of targeting compound, but not erlotinib control (Supplementary Fig. 3c,d, left), while cell viability was unaffected (Supplementary Fig. 3c,d, middle). Unlike with MET and FGFR4, however, AXL and ALK expression level was not altered by compound (Supplementary Fig. 3c,d, right), indicating that the effect of these TKIs on bait interaction with Shc1 is not due to a reduction in receptor protein amount or stability.

Finally, we looked at the more subtle case of whether the reported differential effects of two therapeutic TKIs (erlotinib and osimertinib) on EGFR mutants important in NSCLC could be detected in MaMTH-DS. These included EGFR L858R (responsive to the first-generation TKI erlotinib[18]), EGFR L858R/T790M (which confers resistance to erlotinib, but is sensitive to the third-generation TKI osimertinib[19]), and the recently reported EGFR L858R/T790M/C797S (which is resistant to all current clinically available therapeutic TKIs, including osimertinib)[20]. In agreement with clinical results, erlotinib inhibited interaction of Shc1 with L858R mutant, but not with wild-type (WT) or either drug-resistant mutant, whereas osimertinib affected both L858R and L858R/T790M mutants, but not WT and the C797S triple mutants (Supplementary Fig. 4a). As with the other RTKs tested, these effects were not due to a reduction in reporter cell viability (Supplementary Fig. 4b) and, as with AXL and ALK, no effect of TKIs on bait expression was observed (Supplementary Fig. 4c).

MaMTH-DS screen of drug-resistant EGFR triple mutant. Based on the success of our preliminary assays, we assembled and optimized a high-throughput, automated MaMTH-DS screening

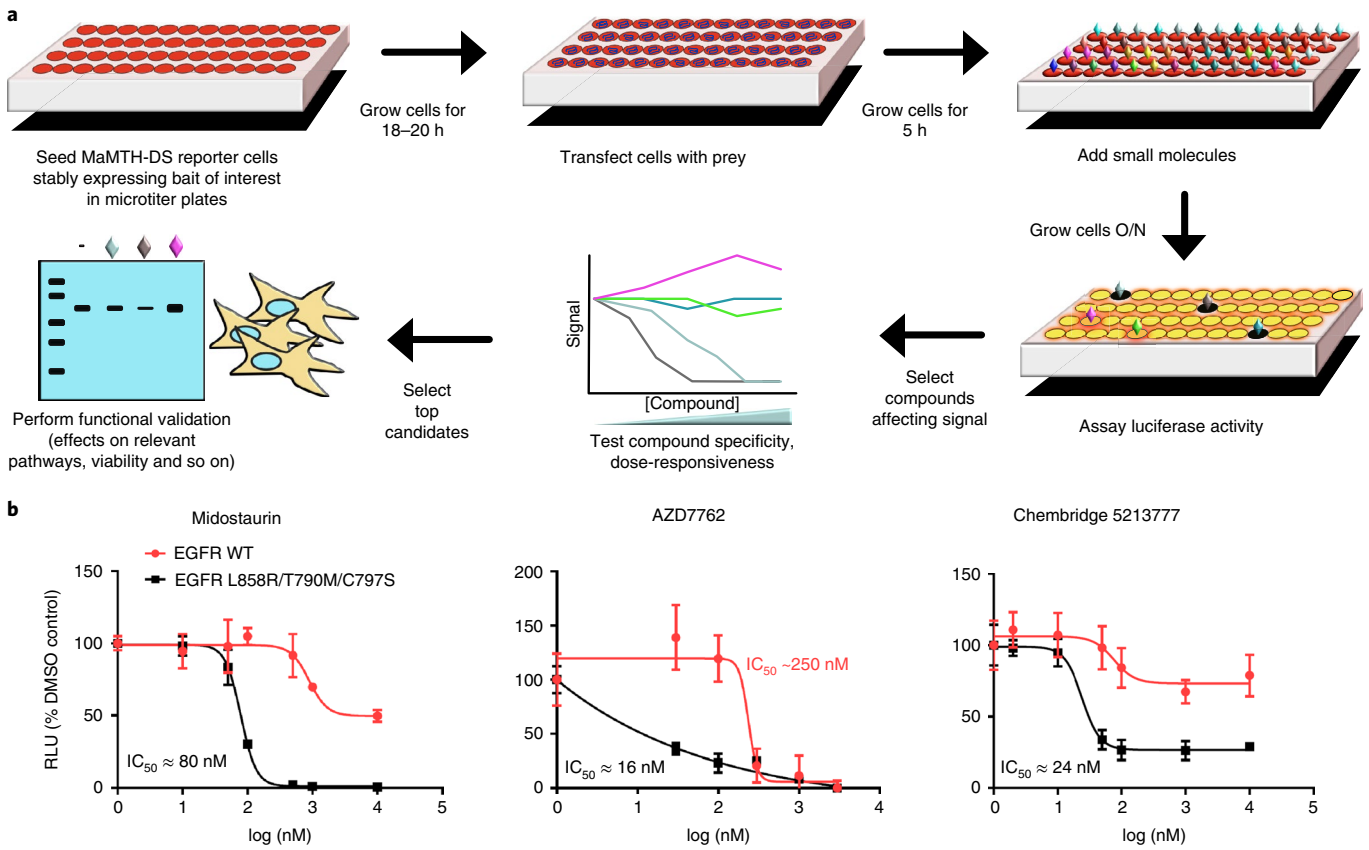

Fig. 1 | Overview of MaMTH-DS platform and top candidates identified in pilot screen. a, Schematic representation of the MaMTH-DS platform workflow. **b**, Dose–response curves for the top three candidate EGFR L858R/T790M/C797S inhibitors (midostaurin, AZD7762 and ChemBridge 5213777) showing robust, dose-responsive and mutant-specific inhibition. Results are shown as the average ± s.d. for three independent experiments.

workflow for rapid detection of small molecules targeting RTK functional interactions (Fig. 1a). To test this new workflow, we performed screening of the clinically relevant, osimertinib-resistant EGFR L858R/T790M/C797S mutant[20] against a pilot library of 2,960 diverse small molecules (Supplementary Fig. 5a and Supplementary Dataset 1). Screening was carried out twice (two independent experiments) to test for reproducibility and was performed using robotics for cell seeding, sample transfection and small-molecule addition. All screen data were subject to Box–Cox power transformation to improve data distribution symmetry and normality before further analysis (Supplementary Fig. 5b). *Z* values across all ten screened plates exceeded 0.5 in the first round of screening (average 0.68 overall). All ten plates exceeded 0.4 (with seven plates exceeding 0.5) in the second round (average 0.56 overall), supporting excellent assay quality[21] (Supplementary Fig. 5c). Data normalization was performed on a per plate basis, using control-based (normalized percentage inhibition, NPI) and sample-based (BScore[22]) approaches, to correct for plate variation and positional effects (Supplementary Fig. 6a). NPI and BScore correlated well, and inhibitory hits were scored using a combined cut-off of greater than 70% NPI and a BScore of −3 or lower (Supplementary Fig. 6b). Overall, we detected a total of 49 candidates from Round 1 and 45 candidates from Round 2, with an overlap of 34 shared hits between both rounds (Supplementary Fig. 6c) and a relatively even distribution of hits across all plates (Supplementary Fig. 7). All raw data for these screens are provided in Supplementary Datasets 2 and 3.

To determine reproducibility and eliminate compounds displaying significant activity against EGFR-WT and/or general toxicity, all 34 shared hits were retested in triplicate using MaMTH-DS, against both EGFR L858R/T790M/C797S and EGFR-WT (Supplementary Table 1). Compounds were selected for further consideration only if they inhibited EGFR L858R/T790M/C797S (but not EGFR-WT) by more than 50% and if the difference in their inhibition of mutant versus WT was both statistically significant and at least two-fold (Supplementary Table 1). The five compounds satisfying these criteria were subjected to dose–response testing from which three (the TKIs midostaurin and AZD7762, and ChemBridge compound 5213777) displayed robust, dose-dependent inhibition of EGFR L858R/T790M/C797S (Fig. 1b), making them candidates for further study.

Functional validation of TKI Hits. Midostaurin (Rydapt) is a multi-kinase inhibitor previously investigated for use against mutant EGFR[23], but its activity has never been shown against EGFR-C797S triple mutant. Notably, the compound has been recently Food and Drug Administration (FDA) approved for treatment of FLT3-mutant acute myeloid leukemia (AML)[24]. Although the kinase inhibitor library used in our collection contains other known, highly specific FLT3 inhibitors (including crenolanib[25], sorafenib[26] and quizartinib[27]), none were found to target the EGFR-C797S triple mutant in our screen (Supplementary Datasets 2 and 3). However, gilteritinib, another next generation TKI recently approved by the FDA for treatment of FLT3-mutant AML[28], was absent from our library. Secondary testing of this compound in MaMTH-DS found that, despite considerable structural differences with midostaurin (Supplementary Fig. 8a), it is also a potent and highly specific inhibitor of the EGFR triple mutant (Supplementary Fig. 8b). We therefore decided to include gilteritinib in our validation studies.

We first examined the activity of midostaurin and gilteritinib using in vitro kinase assays with recombinant kinase domain from

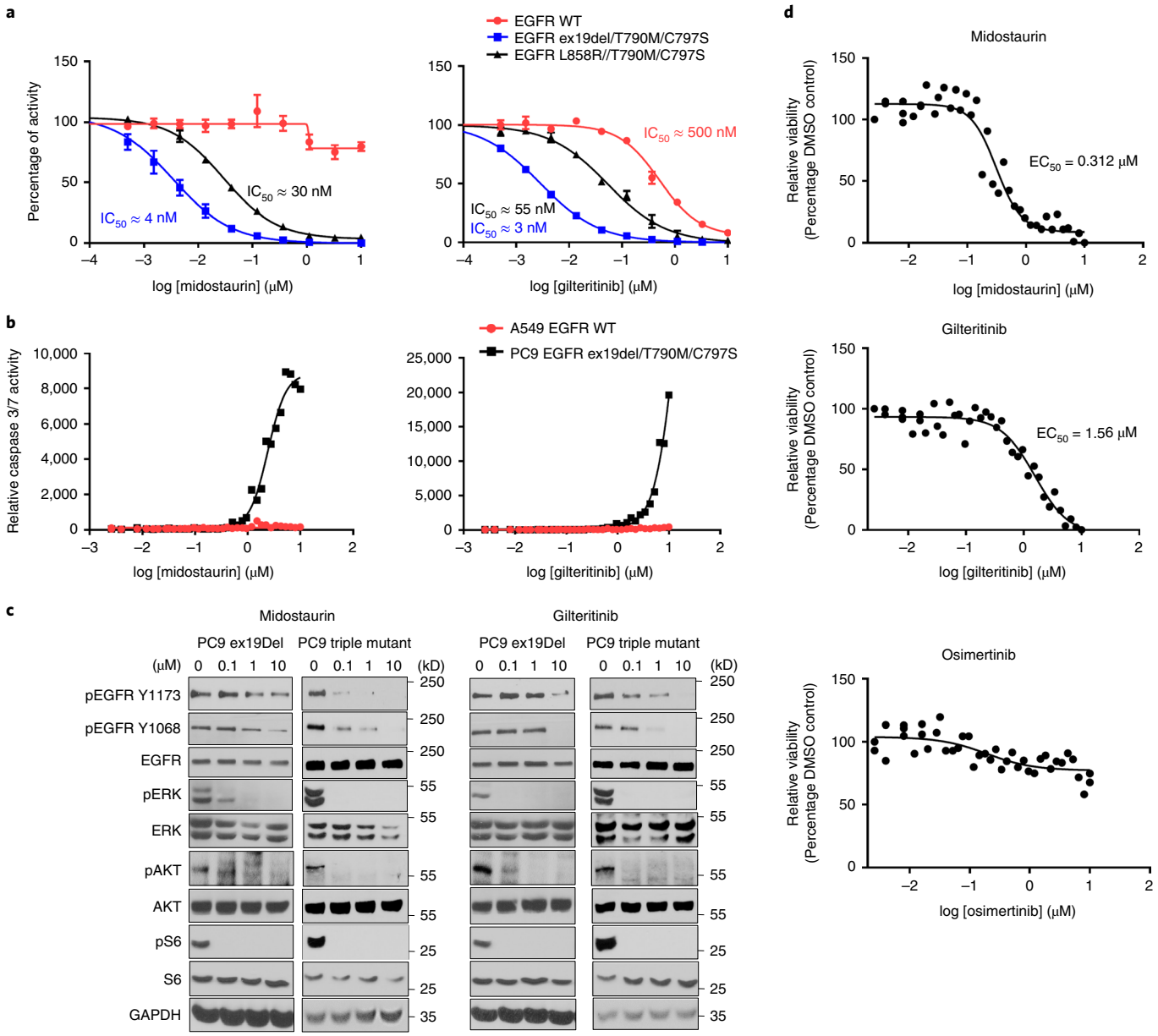

Fig. 2 | Validation of midostaurin and gilteritinib as EGFR ex19del/T790M/C797S and EGFR L858R/T790M/C797S activating mutant inhibitors. **a**, In vitro kinase assay of recombinant kinase domain (residues 696–1,022) of indicated mutant or WT EGFR in the presence of midostaurin (left) or gilteritinib (right). Results are shown as the average ± s.d. for two independent experiments. **b**, Effect of midostaurin and gilteritinib on caspase 3/7 activity in PC9 EGFR ex19del/T790M/C797S and A549 EGFR-WT cells. Results are shown as single 36-point dose–response experiments. **c**, Effects of midostaurin (left) and gilteritinib (right) on EGFR activation and downstream signaling in PC9 EGFR ex19del and EGFR ex19del/T790M/C797S cells after 2 h treatment (see Supplementary Figs. 21–24 for source blot images). Results are representative of at least two independent experiments. **d**, Midostaurin and gilteritinib mediated reduction of PC9 EGFR ex19del/T790M/C797S organoid viability. Osimertinib control, which does not target triple-mutant EGFR activity, has no effect. Results are shown as single 36-point dose–response experiments.

EGFR-C797S triple mutants. These included the EGFR L858R/T790M/C797S mutant used in our screen and the other commonly occurring, drug-resistant, NSCLC mutant ex19del/T790M/C797S. Both midostaurin and gilteritinib directly inhibited the kinase domain of EGFR-C797S triple mutants with IC_{50} values in the low nanomolar range (at 100 μM ATP), displaying significantly more potent activity toward the mutants than WT EGFR (Fig. 2a and Supplementary Table 2). We also assessed the effect of midostaurin and gilteritinib on recombinant oncogenic EGFR single and double mutants using in vitro kinase assays, and found that both compounds were less effective against L858R and ex19del single mutants, but displayed moderate to strong activity against the ex19del/T790M and L858R/T790M double mutants (with slightly greater potency observed for midostaurin), indicating their activity is not restricted to the triple oncogenic mutants alone (Supplementary Table 2).

We next looked at the effects of midostaurin and gilteritinib in cancer cell lines. Both compounds induced caspase 3 and 7 activity in PC9 adenocarcinoma cells carrying EGFR ex19del/T790M/C797S triple mutant, but not in A549 epithelial cells carrying EGFR-WT (Fig. 2b). Midostaurin and gilteritinib also reduced EGFR phosphorylation/activation in PC9-ex19del/T790M/C797S triple-mutant cells more strongly than in PC9-ex19del single mutant background cells (Fig. 2c). Phosphorylation of downstream signaling partners was also affected, although more subtly than EGFR

phosphorylation, with midostaurin more potently reducing pAKT and pERK levels and gilteritinib more potently reducing pAKT levels in triple-mutant cells (Fig. 2c). This more subtle effect is likely due to midostaurin and gilteritinib having modest activity toward single mutant EGFR (Supplementary Table 2) and possibly targeting additional signaling pathway kinases. Midostaurin and gilteritinib also potently affected the growth of PC9 triple-mutant organoids, in contrast to osimertinib control that does not target the activity of EGFR ex19del/T790M/C797S (Fig. 2d).

The remaining TKI identified in our screen, AZD7762, is a CHK1/2 kinase inhibitor that has not been reported as active against EGFR NSCLC mutants, but has been the subject of numerous studies, including a Phase 1 clinical trial for treatment of solid tumors; however, work was discontinued due to cardiac toxicity[29,30]. Analysis of activity by in vitro kinase assay using recombinant EGFR-WT, EGFR ex19del/T790M/C797S and EGFR L858R/T790M/C797S proteins revealed that AZD7762 effectively inhibited the kinase activity of all three forms of EGFR, and was most potent against the ex19del triple mutant, with an IC_{50} of 10 nM at 100 µM ATP (Supplementary Fig. 9). However, AZD7762 activity toward WT and L858R triple mutants was comparable (with IC_{50} values of 240 and 280 nM, respectively) in contrast to the differential effect on the interaction of Shc1 with EGFR-WT and mutant observed in MaMTH-DS (IC_{50} values of 250 and 16 nM, respectively). While these data are interesting and indicate involvement of additional cellular factors in the mutant-specificity observed in MaMTH-DS, the compound still displays substantial activity toward WT. Based on this, as well as AZD7762's previously described toxicity and detailed coverage in the literature, we decided not to pursue further validation of this compound.

Functional validation of ChemBridge 5213777 (EMI1). Our final hit, ChemBridge 5213777 (3-(1,3-benzoxazol-2-yl)-7-(diethylamino)-2H-chromen-2-one), which we have renamed EMI1 (EGFR MaMTH Inhibitor) (**1**) (Fig. 3a), is a coumarin derivative. Although published information on EMI1 is limited, previous studies have shown it displays anti-proliferative activity against various cancer cell lines and potential inhibitory effects on microtubule dynamics[31]. EMI1, while potently reducing the interaction of EGFR triple mutant with Shc1 in our MaMTH-DS assay, did not behave as a TKI and displayed no inhibition of the kinase activity of EGFR triple-mutant protein in vitro (Fig. 3b). EMI1 did, however, more strongly inhibit the viability and increase the caspase 3/7 activity of PC9 EGFR ex19del/T790M/C797S triple-mutant cells than noncancerous human bronchial epithelial (HBE) cells (Fig. 3c,d), as well as potently reduce PC9 EGFR ex19del/T790M/C797S organoid viability (Fig. 3e). Notably, EMI7 (**2**), a structurally similar analog lacking the diethylamino group, obtained as part of our effort to identify molecular regions important in compound activity and eliminate functional groups associated with potential in vivo toxicity (Supplementary Fig. 10a), had no effect on the interaction of EGFR triple mutant with Shc1 (Supplementary Fig. 10b) or on PC9 triple-mutant cell or organoid viability (Supplementary Fig. 10c,d). This indicates an important role for the diethylamino group in EMI1 activity. We decided to use EMI7 as a control in our functional studies of EMI1.

To investigate the EMI1 mechanism of action we first examined its reported activity as a microtubule-targeting agent. Using human embryonic kidney 293 (HEK293) MaMTH reporter EGFR stable cells expressing fluorescently tagged microtubule plus-end binding protein EB3, we showed that EMI1 had a similar inhibitory effect on microtubule plus-end growth in both EGFR-WT and EGFR-C797S triple-mutant cells at 50–100 nM concentration (Fig. 3f). At 1 µM concentration, EMI1 strongly depolymerized interphase microtubules, perturbed spindle formation and induced strong mitotic block in PC9 EGFR ex19del/T790M/C797S cells after 20 h of treatment (Supplementary Fig. 11). Furthermore, in vitro microtubule dynamics assays using purified tubulin and mCherry-EB3 showed that EMI1 reduced microtubule growth rate and time, while increasing catastrophe frequency (Supplementary Fig. 12). The inactive EMI7 derivative had no effect on microtubule dynamics (Supplementary Fig. 12). Together these results show that EMI1 directly targets microtubules. However, EMI1 displayed an effect on EGFR activation and signaling through extracellular signal-regulated kinase (ERK) and protein kinase B (AKT) in PC9 EGFR ex19del/T790M/C797S cells (at a 20 µM concentration) that was not evident when using other microtubule destabilizing compounds including Rigosertib, Nocodazole and Colchicine, or the microtubule-stabilizer Docetaxel. Thus, EMI1 appears to have a unique mutant EGFR-specific polypharmacology (Fig. 3g).

We next used MaMTH-DS to determine whether EMI1 activity toward EGFR is due to direct and specific inhibition of its physical interaction with Shc1. To this end, we examined interaction of EGFR L858R/T790M/C797S bait with two other functionally important EGFR-binding partners CrkII and Hsp90. EMI1 inhibited interaction of both proteins with EGFR at a level similar to that observed with Shc1 (Supplementary Fig. 13), indicating it is not a specific inhibitor of the EGFR-Shc1 PPI interface. Rather, the loss of interaction mediated by EMI1 appears to be due to a more general alteration in EGFR activity.

Next, we assessed the effect of EMI1 on additional NSCLC cells including PC9 cells expressing either EGFR ex19del or EGFR ex19del/T790M and A549 EGFR-WT cells. EMI1 induced EGFR degradation, and inhibited the activation of EGFR, ERK, AKT and S6 in PC9-ex19del and PC9-ex19del/T790M cells (Supplementary Fig. 14a). EGFR activation was not affected in A549 cells, but there was a modest decrease in total EGFR levels and attenuation of downstream signaling components ERK, AKT and S6 (Supplementary Fig. 14b). These data indicate that there is a differential response to EMI1 with respect to EGFR activation between WT and mutant EGFR, where mutant EGFR activation is decreased.

Fig. 3 | Validation of EMI1 as an EGFR ex19del/T790M/C797S and EGFR L858R/T790M/C797S activating mutant inhibitor. a, Chemical structure for EMI1. **b**, In vitro kinase assay of recombinant kinase domain (residues 696–1,022) of indicated mutant or WT EGFR in the presence of EMI1. Results are shown as the average ± s.d. for two independent experiments. **c**, Effect of EMI1 on the viability of PC9 EGFR ex19del/T790M/C797S and HBE bronchial epithelial lung EGFR-WT control cells. Results are shown as the average ± s.d. for three independent experiments. **d**, Effect of EMI1 on caspase 3/7 activity in PC9 EGFR ex19del/T790M/C797S and HBE EGFR-WT cells. Results are shown as single 36-point dose–response experiments. **e**, Viability assay measuring effect of EMI1 on PC9 EGFR ex19del/T790M/C797S organoid growth. Results are shown as single 36-point dose–response experiments. **f**, Maximum intensity projections (stream acquisition/exposure time 500 ms/100 frames) showing the effect of EMI1 on microtubule dynamics in HEK293 MaMTH reporter cells stably expressing EGFR-WT or EGFR L858R/T790M/C797S transfected with EB3-TagRFP as a microtubule plus-end marker. The contrast is inverted. Graph shows quantification of microtubule plus-end velocity in HEK293 reporter cells for EMI1. $n = 51, 41, 36$ for HEK293 EGFR-WT, control, 50 and 100 nM. $n = 49, 47, 41$ for HEK293 EGFR-C797S control, 50 and 100 nM. Significant P values are displayed and were calculated using the Mann–Whitney test. **g**, Western blot analysis showing activity of EMI1 and other microtubule-targeting compounds after 2 h treatment on EGFR ex19del/T790M/C797S activation and downstream signaling in PC9 triple-mutant cells (see Supplementary Fig. 25 for source blot images). Results are representative of at least two independent experiments.

It is well established that changes in receptor internalization, recycling and degradation affect the signaling response and can contribute to tumorigenesis[32]. In addition, the concentration of active (phosphorylated) RTK in early endosomes and the number of early endosomes containing phosphorylated RTK regulate signaling amplitude and duration[33]. Molecules targeting EGFR may

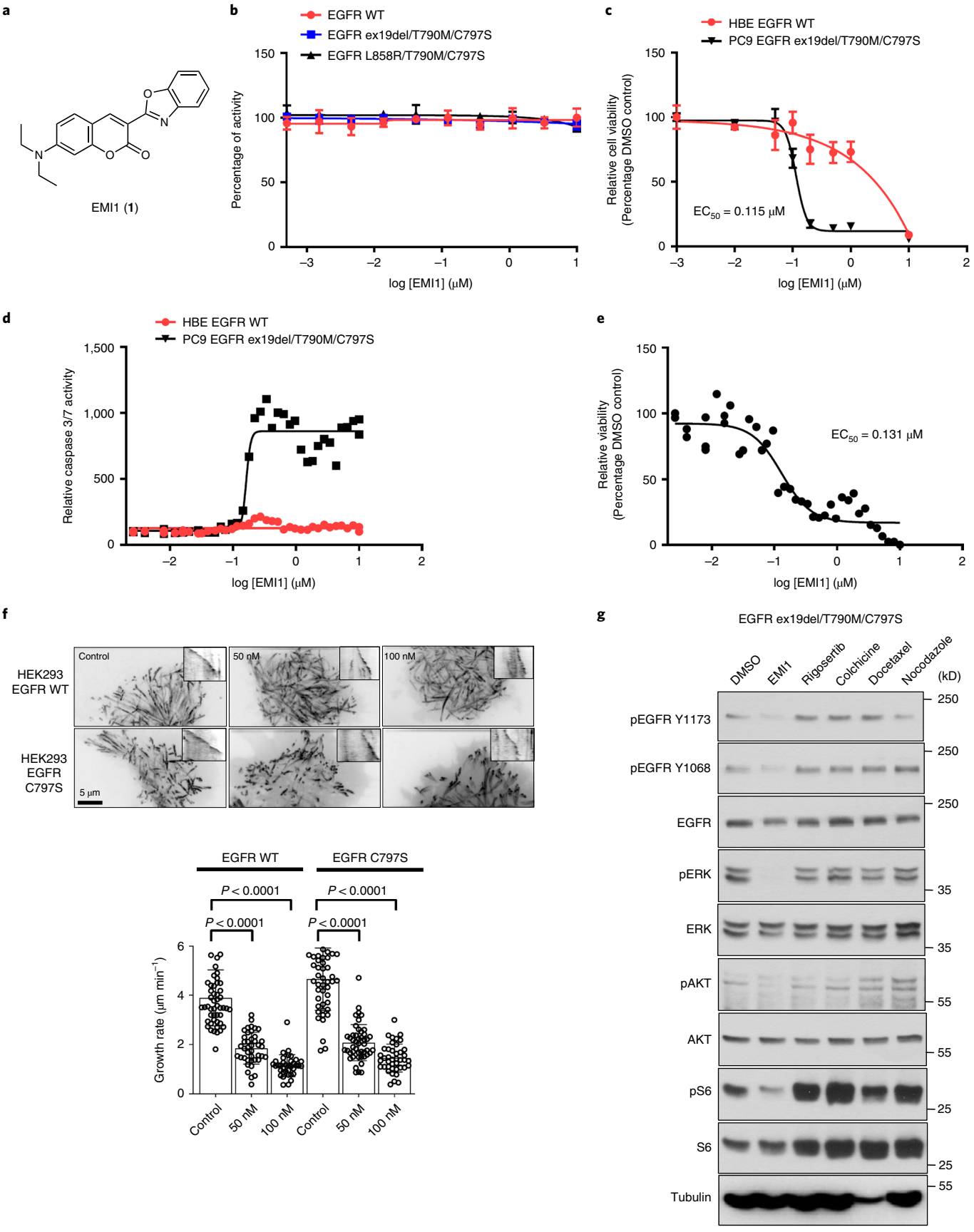

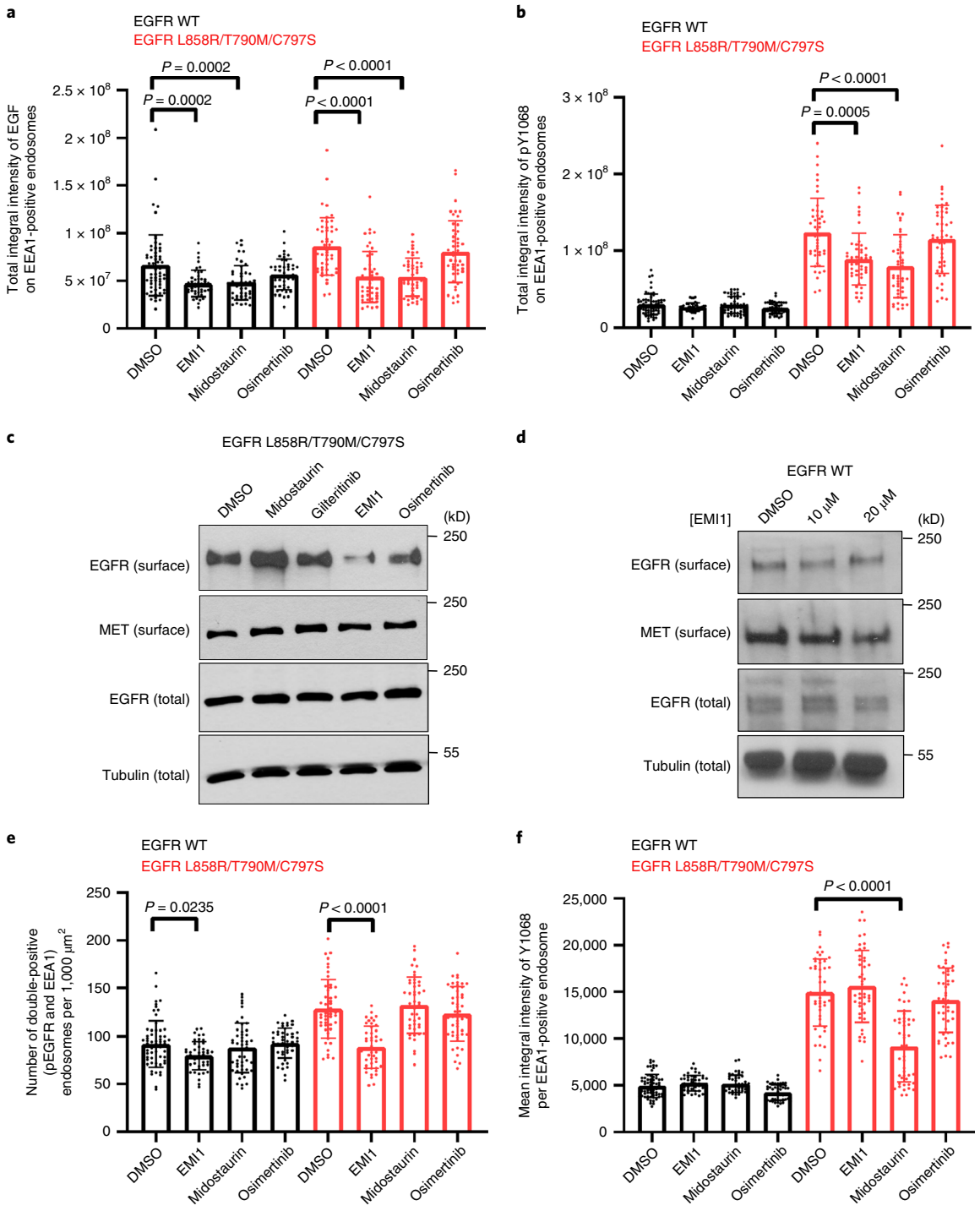

Fig. 4 | Investigating effect of EMI1 on activated EGFR L858R/T790M/C797S endosomal trafficking. a, Total integral intensity of EGF on EEA1-positive endosomes normalized on cytoplasm area after 30 min of EGF stimulation on 1 μM compound treatment in HEK293 EGFR-WT cells or EGFR L858R/T790M/C797S cells. **b**, Total integral intensity of pY1068 on EEA1-positive endosomes normalized on cytoplasm area after 30 min of EGF stimulation with 1 μM compound treatment in HEK293 EGFR-WT cells or EGFR L858R/T790M/C797S cells. Results are shown as dot plots representing the average ± s.d. For EGFR-WT cells, $n = 63$, 46, 48 and 48 images were analyzed for DMSO, EMI1, midostaurin and osimertinib treatment, respectively. For EGFR-C797S cells, $n = 48$, 46, 46, 48 images were analyzed for DMSO, EMI1, midostaurin and osimertinib treatment, respectively. Significant *P* values are displayed and were calculated using Dunn's multiple comparison test. **c**, Cell surface biotinylation assay assessing surface levels of EGFR L858R/T790M/C797S after treatment with 5 μM compound for 2 h. Results are representative of at least two independent experiments. **d**, Cell surface biotinylation assay assessing surface levels of EGFR-WT after treatment with EMI1 for 2 h. Results are representative of at least two independent experiments (see Supplementary Fig. 26 for source blot images). **e**, Number of pEGFR and EEA1 double-positive endosomes per 1,000 μm^2 after 30 min stimulation by EGF. **f**, Mean integral intensity of pEGFR on double-positive (pEGFR and EEA1) endosomes after 30 min stimulation by EGF. Results are shown as dot plots representing the average ± s.d. For EGFR-WT cells, $n = 63$, 46, 48 and 48 images were analyzed for DMSO, EMI1, midostaurin and osimertinib treatment, respectively. For EGFR-C797S cells, $n = 48$, 46, 46, 48 images were analyzed for DMSO, EMI1, midostaurin and osimertinib treatment, respectively. Significant *P* values are displayed and were calculated using Dunn's multiple comparison test.

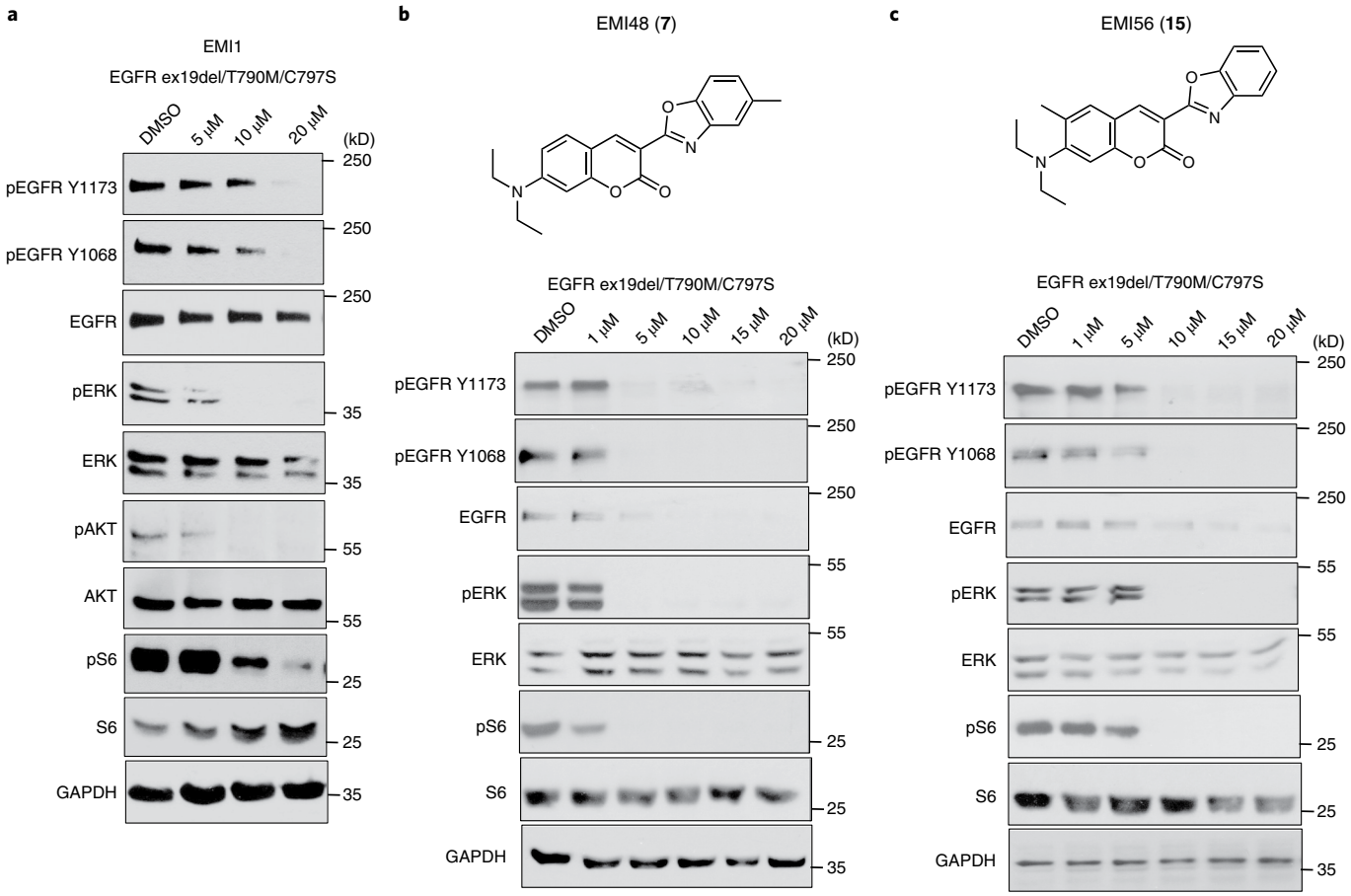

Fig. 5 | Generation and testing of EMI1 chemical analogs. a–c, Western blot analysis showing effects of EMI1 (**a**), EMI48 (**b**) and EMI56 (**c**) on total EGFR levels, activation and downstream signaling after 2 h of treatment in PC9 EGFR ex19del/T790M/C797S cells (see Supplementary Figs. 27 and 28 for source blot images). Results are representative of at least two independent experiments.

thus result in alterations of endosomal trafficking that could in turn feed back on its activity. We therefore assessed whether EMI1, as well as midostaurin and osimertinib for comparison, affect EGFR endosomal trafficking, in terms of kinetics and endosomal distribution, using an automated microscopy approach. HEK293 MaMTH reporter EGFR-WT and EGFR L858R/T790M/C797S cells were incubated with fluorescently labeled EGF for 30 min plus or minus 1 μM compound, fixed and stained with antibodies against the early endosomal marker EEA1 to label early endosomes, and anti-EGFR pY1068 to label phosphorylated pEGFR, as previously described[33]. Representative images for trafficking assays are provided in Supplementary Figs. 15 and 16. We found that EMI1, like midostaurin, significantly reduced EGF accumulation in EEA1-positive early endosomes in EGFR L858R/T790M/C797S cells, in contrast to osimertinib that had no effect (Fig. 4a, red). A similar effect was observed for EGFR-WT cells but to a lesser degree (Fig. 4a, black). EMI1 and midostaurin, but not osimertinib, also significantly reduced the overall amount of EGFR pY1068 localized to EEA1-positive endosomes in EGFR L858R/T790M/C797S, but not in EGFR-WT, cells (Fig. 4b). These results indicate that EMI1 and midostaurin exert an inhibitory effect on the uptake and distribution of activated, mutant EGFR receptor in early endosomes.

The inhibition of EGF uptake may be due to lower cell surface levels of EGFR. Indeed, EMI1 treatment for 2 h led to a marked decrease in surface levels of EGFR in mutant cells (Fig. 4c), an effect not observed on midostaurin or osimertinib treatment or in cells carrying wild-type EGFR (Fig. 4d). Total levels of EGFR did not change in the mutant or WT EGFR expressing cells. Also, no changes occurred in the surface level of another RTK, c-MET. These results argue that EMI1 and midostaurin exert their effects on uptake of EGF by different mechanisms.

EMI1 treatment also decreased the number of early endosomes carrying activated EGFR L858R/T790M/C797S to levels similar to wild-type cells (Fig. 4e) but did not affect the average amount of activated EGFR per endosome (Fig. 4f). Conversely, midostaurin reduced the amount of activated EGFR per endosome (Fig. 4f) but had no effect on total endosome number (Fig. 4e), consistent with its activity as a direct inhibitor of mutant EGFR kinase activity (and therefore endosomal internalization). These observations have important consequences for the modulatory activity of EMI1 on the signaling of the EGFR L858R/T790M/C797S mutant.

Medicinal chemistry analysis of EMI1. To improve potency of EMI1 and explore the chemical groups involved in its function, we performed medicinal chemistry to modify the structure of the compound. Our strategy involved breaking the molecule into three groups: the diethylamino substituent, the coumarin backbone and the benzoxazole substituent. We generated 17 derivatives (3–19) (Supplementary Fig. 17) and tested each for their ability to reduce PC9 EGFR ex19del/T790M/C797S cell viability (Supplementary Fig. 18) and affect EGFR triple-mutant activation and downstream signaling (at a 10 μM dose) in PC9 EGFR ex19del/T790M/C797S cells (Supplementary Fig. 19). We identified two derivatives, EMI48 (**7**) and EMI56 (**15**), displaying greater potency toward mutant EGFR than EMI1. These contain an additional methyl group on either the benzoxazole ring (EMI48) or coumarin backbone

(EMI56). Dose–response experiments showed EMI48 more strongly inhibited total EGFR levels, activation and downstream signaling than EMI1, with effects observed at a 5 μM concentration, compared to the 20 μM required for EMI1 (Fig. 5a,b). EMI56 also displayed an enhanced effect, but at the 10 μM level (Fig. 5c). Unlike EMI1, EMI48 and EMI56 did not affect interphase microtubules, or have an effect on spindle formation in PC9 EGFR ex19del/T790M/C797S cells (Supplementary Fig. 20), indicating that the microtubule and EGFR-targeting activity of EMI1 are distinct. Both analogs warrant further investigation to better understand the mechanism involved in their activity and increased potency.

Discussion

We developed MaMTH-DS, a powerful drug discovery platform for rapid, high-throughput identification of small molecules modulating interactions between full-length RTKs and functional partner proteins such as Shc1 or other relevant EGFR phospho-binding proteins, directly in living cells, with the benefit that identified small-molecule candidates have already passed cell permeability and toxicity tests. We applied this method to examine and identify specific modulators of disease-associated RTKs. Preliminary testing of MaMTH-DS using various RTK baits associated with cancer, including MET, FGFR4, AXL, ALK and EGFR, revealed highly specific, dose-dependent reduction in reporter activity in response to known targeting compounds in all cases. Results closely mirrored those observed in a clinical setting, demonstrating the robustness of MaMTH-DS as a drug discovery tool. Notably, our results indicated that compound effects on the functional interaction of the RTK baits with adapter protein was mediated by distinct mechanisms, with MET and FGFR4 interactions modulated at least in part by changes in protein level.

Full proof-of-principle MaMTH-DS screening of a pilot collection of 2,960 small molecules identified three new compounds (midostaurin, AZD7762 and EMI1) specifically targeting the EGFR L858R/T790M/C797S triple mutant associated with drug-resistant NSCLC. Additionally, based on functional similarities with midostaurin, we identified the TKI gilteritinib as a fourth EGFR triple-mutant-targeting compound. The potency and specificity of these molecules were successfully validated in follow-up studies using the both biochemical assays and the NSCLC PC9 EGFR ex19del/T790M/C797S lung adenocarcinoma cell line and associated organoid model, indicating that all may be of value in further research and therapeutic development. Midostaurin and gilteritinib, in particular, both of which were recently FDA approved for use in the treatment of FLT3-mutant AML, could potentially be repurposed for treatment of patients suffering from EGFR L858R/T790M/C797S and EGFR ex19del/T790M/C797S associated NSCLC and, as such, are currently the subject of clinical studies.

Importantly, neither AZD7762 nor EMI1 would have been detected as mutant-specific inhibitors of our target bait by in vitro kinase assay; AZD7762 because (although a TKI) its specificity toward mutant EGFR appears to depend on additional factors present in the live-cell format, and EMI1 because it employs a new mechanism of action distinct from direct kinase inhibition. Our discovery of both of these compounds highlights the potential advantages of using MaMTH-DS alongside conventional assays.

The unique mode of action of EMI1 will be the focus of future studies. Thus far, we identified two distinct activities for EMI1: a direct effect on microtubule polymerization and an indirect effect on mutant EGFR signaling and trafficking. Chemical separation of these activities will be essential for follow-up studies and potential therapeutic applications. Analysis of the effect of EMI1 on the endosomal distribution of EGFR has provided important first clues about its mutant EGFR-specific activity. Investigating the nature of this specific activity should be invaluable in identifying new mechanisms for targeting oncogenic EGFR and potentially other RTK receptors. Further work will focus on in-depth monitoring of mutant movement throughout the endosomal pathway, examining potential changes in late endosomal representation and lysosomal degradation in response to EMI1 treatment. Additionally, the dual role of EMI1 as a microtubule destabilizer and modulator of mutant EGFR endosomal distribution will be explored to better understand how EMI1 mediates both effects, taking into account the impact of drug dosages and treatment times. We will also expand our medicinal chemistry studies, performing more thorough characterization of our current compound set, as well as preparing additional analogs. The generation of two derivatives, EMI48 and EMI56, which displayed greater potency toward mutant EGFR signaling than EMI1 and a reduced microtubule-depolymerization activity represents a useful step in this direction. These and future analogs will also be studied in further depth in animal models to better understand their mode of action and therapeutic potential.

Collectively, our data illustrate the ability of the live-cell MaMTH-DS assay to sensitively detect the loss of functional interactions in response to diverse, but specific, effects of drug action, via mechanisms that may not be detectable by conventional in vitro kinase screening approaches. Specifically, MaMTH-DS can theoretically identify several classes of RTK inhibitors that lead to reduced binding of a functional protein partner including (1) direct inhibitors of RTK enzymatic activity (such as midostaurin and gilteritinib); (2) direct physical inhibitors of PPIs; (3) inhibitors that affect RTK dimerization; (4) allosteric inhibitors of RTK enzymatic activity and (5) inhibitors that affect EGFR trafficking. In this way, our platform represents a potent new drug discovery tool that can complement conventional in vitro biochemical assays for drug screening of RTKs such as EGFR. The highly sensitive and flexible nature of the technology also make it amenable for use with other integral membrane protein targets, potentially expanding its use beyond RTKs. The MaMTH-DS platform represents a technical advance in the area of drug screening research that should greatly facilitate the identification of valuable new therapeutic molecules.

Online content

Any methods, additional references, Nature Research reporting summaries, source data, extended data, supplementary information, acknowledgements, peer review information; details of author contributions and competing interests; and statements of data and code availability are available at https://doi.org/10.1038/s41589-020-0484-2.

Received: 18 October 2017; Accepted: 27 January 2020;
Published online: 24 February 2020

References

1. Lemmon, M. A. & Schlessinger, J. Cell signaling by receptor tyrosine kinases. *Cell* **141**, 1117–1134 (2010).
2. Volinsky, N. & Kholodenko, B. N. Complexity of receptor tyrosine kinase signal processing. *Cold Spring Harb. Perspect. Biol.* **5**, a009043–a009043 (2013).
3. Jia, Y., Quinn, C. M., Kwak, S. & Talanian, R. V. Current in vitro kinase assay technologies: the quest for a universal format. *Curr. Drug Discov. Technol.* **5**, 59–69 (2008).
4. Petschnigg, J. et al. The mammalian-membrane two-hybrid assay (MaMTH) for probing membrane-protein interactions in human cells. *Nat. Methods* **11**, 585–592 (2014).
5. Sokolina, K. et al. Systematic protein–protein interaction mapping for clinically relevant human GPCRs. *Mol. Syst. Biol.* **13**, 918 (2017).
6. Snider, J. et al. Mapping the functional yeast ABC transporter interactome. *Nat. Chem. Biol.* **9**, 565–572 (2013).
7. Stagljar, I., Korostensky, C., Johnsson, N. & te Heesen, S. A genetic system based on split-ubiquitin for the analysis of interactions between membrane proteins in vivo. *Proc. Natl Acad. Sci. USA* **95**, 5187–5192 (1998).
8. Yao, Z. et al. A global analysis of the receptor tyrosine kinase-protein phosphatase interactome. *Mol. Cell* **65**, 347–360 (2017).
9. Petschnigg, J. et al. Systematic identification of oncogenic EGFR interaction partners. *J. Mol. Biol.* **429**, 280–294 (2017).

10. Robbins, A. K. & Horlick, R. A. Macrophage scavenger receptor confers an adherent phenotype to cells in culture. *Biotechniques* **25**, 240–244 (1998).
11. Zheng, Y. et al. Temporal regulation of EGF signalling networks by the scaffold protein Shc1. *Nature* **499**, 166–171 (2013).
12. Saucier, C. et al. The Shc adaptor protein is critical for VEGF induction by Met/HGF and ErbB2 receptors and for early onset of tumor angiogenesis. *Proc. Natl Acad. Sci. USA* **101**, 2345–2350 (2004).
13. Goździk-Spychalska, J. et al. C-MET inhibitors in the treatment of lung cancer. *Curr. Treat. Options Oncol.* **15**, 670–682 (2014).
14. Hagel, M. et al. First selective small molecule inhibitor of FGFR4 for the treatment of hepatocellular carcinomas with an activated FGFR4 signaling pathway. *Cancer Discov.* **5**, 424–437 (2015).
15. Eder, J. P. et al. A phase I study of foretinib, a multi-targeted inhibitor of c-Met and vascular endothelial growth factor receptor 2. *Clin. Cancer Res.* **16**, 3507–3516 (2010).
16. Qian, F. et al. Inhibition of tumor cell growth, invasion, and metastasis by EXEL-2880 (XL880, GSK1363089), a novel inhibitor of HGF and VEGF receptor tyrosine kinases. *Cancer Res.* **69**, 8009–8016 (2009).
17. Zhang, S. et al. The potent ALK inhibitor brigatinib (AP26113) overcomes mechanisms of resistance to first- and second-generation ALK inhibitors in preclinical models. *Clin. Cancer Res.* **22**, 5527–5538 (2016).
18. Walter, A. O. et al. Discovery of a mutant-selective covalent inhibitor of EGFR that overcomes T790M-mediated resistance in NSCLC. *Cancer Discov.* **3**, 1404–1415 (2013).
19. Jiang, T. & Zhou, C. Clinical activity of the mutant-selective EGFR inhibitor AZD9291 in patients with EGFR inhibitor-resistant non-small cell lung cancer. *Transl. Lung Cancer Res.* **3**, 370–372 (2014).
20. Thress, K. S. et al. Acquired EGFR C797S mutation mediates resistance to AZD9291 in non-small cell lung cancer harboring EGFR T790M. *Nat. Med.* **21**, 560–562 (2015).
21. Zhang, J.-H., Chung, T. D. & Oldenburg, K. R. A simple statistical parameter for use in evaluation and validation of high throughput screening assays. *J. Biomol. Screen.* **4**, 67–73 (1999).
22. Brideau, C., Gunter, B., Pikounis, B. & Liaw, A. Improved statistical methods for hit selection in high-throughput screening. *J. Biomol. Screen.* **8**, 634–647 (2003).
23. Lee, H. J. et al. Noncovalent wild-type-sparing inhibitors of EGFR T790M. *Cancer Discov.* **3**, 168–181 (2013).
24. M., L. Midostaurin approved for FLT3-mutated AML. *Blood* **129**, 3403–3406 (2017).
25. Galanis, A. et al. Crenolanib is a potent inhibitor of FLT3 with activity against resistance-conferring point mutants. *Blood* **123**, 94–100 (2014).
26. Antar, A. et al. Inhibition of FLT3 in AML: a focus on sorafenib. *Bone Marrow Transplant.* **52**, 344–351 (2017).
27. Cortes, J. et al. Quizartinib, an FLT3 inhibitor, as monotherapy in patients with relapsed or refractory acute myeloid leukaemia: an open-label, multicentre, single-arm, phase 2 trial. *Lancet Oncol.* **19**, 889–903 (2018).
28. Perl, A. E. et al. Selective inhibition of FLT3 by gilteritinib in relapsed or refractory acute myeloid leukaemia: a multicentre, first-in-human, open-label, phase 1–2 study. *Lancet Oncol.* **18**, 1061–1075 (2017).
29. Zabludoff, S. D. et al. AZD7762, a novel checkpoint kinase inhibitor, drives checkpoint abrogation and potentiates DNA-targeted therapies. *Mol. Cancer Ther.* **7**, 2955–2966 (2008).
30. Sausville, E. et al. Phase I dose-escalation study of AZD7762, a checkpoint kinase inhibitor, in combination with gemcitabine in US patients with advanced solid tumors. *Cancer Chemother. Pharmacol.* **73**, 539–549 (2014).
31. Kim, S. N. et al. 7-Diethylamino-3(2′-benzoxazolyl)-coumarin is a novel microtubule inhibitor with antimitotic activity in multidrug resistant cancer cells. *Biochem. Pharmacol.* **77**, 1773–1779 (2009).
32. Mellman, I. & Yarden, Y. Endocytosis and cancer. *Cold Spring Harb. Perspect. Biol.* **5**, a016949 (2013).
33. Villaseñor, R., Nonaka, H., Del Conte-Zerial, P., Kalaidzidis, Y. & Zerial, M. Regulation of EGFR signal transduction by analogue-to-digital conversion in endosomes. *eLife* **4**, e06156 (2015).

Methods

MaMTH assays. Cells stably expressing bait of interest (EGFR, MET) were seeded into 96-well TC-treated plates and grown at 37 °C/5% CO_2 overnight in DMEM/10% FBS/1% PS to ~50–60% confluency. Cells were transfected with 50 ng per well of Nub-Shc1 'prey' protein by calcium phosphate precipitation. Five hours after transfection, media was aspirated out and cells were treated with 100 µl of fresh media containing specific compound and 0.5 µg ml^{-1} of tetracycline to induce bait expression. After 24 h, luciferase activity was measured by chemiluminescence.

Western analysis of bait and downstream signaling molecule expression and phosphorylation. Cells grown under the specified conditions were washed with ice-cold PBS before addition of the cell lysis buffer 10× (Cell Signalling Technology, no. 9803) supplemented with protease inhibitors. Lysates were transferred to 1.5 ml microtubes, and centrifuged for 16,000*g* for 10 min. The supernatants were mixed with Laemmli sample buffer, and boiled at 95 °C for 5 min. Protein quantification was performed using the BCA Protein Assay Reagent (Pierce) according to the manufacturer's protocol before addition of the sample buffer. Western blot analyses were performed after separation by SDS–PAGE and transferred to nitrocellulose membranes. The membranes were then blocked with 2% BSA in Tris-buffered saline/Tween 20 (TBS-T). Antibodies used for western blot analysis were: phospho-EGFR antibody (Tyr1173; Santa Cruz, sc101668, 1:10,000), total EGFR (Cell Signalling Technology, no. 4267, 1:10,000), phospho-AKT (Ser473; Cell Signalling Technology, no. 4060, 1:10,000), total AKT (Cell Signalling Technology, no. 4691, 1:10,000), phospho-ERK (Thr202/Tyr204; Cell Signalling Technology, no. 9101, 1:10,000), total ERK1/2 (Cell Signalling Technology, no. 9102, 1:10,000), phospho-S6 (Ser240/244, Cell Signalling Technology, no. 5364, 1:10,000), total S6 (Cell Signalling Technology, no. 5364, 1:10,000), anti-GAPDH (Santa Cruz, 1:10,000), anti-tubulin (Santa Cruz, 1:10,000) or anti-V5 (Cell Signalling Technology, 1:10,000).

Cell viability assays. MaMTH stable bait cells, PC9 or HBE cells were seeded into 96-well plates at 10,000 cells per well. For MaMTH stable cells, the cells were treated the next day with each inhibitor in a dose-dependent manner in addition to 0.5 µg ml^{-1} tetracycline to induce bait expression. For PC9 and HBE cells, the cells were treated with each compound the same day as seeding. After 72 h of drug treatment, cell viability was measured using the CellTiter-Glo assay (Promega).

EGFR localization and trafficking analyses. The experiment was performed in 384-well CellCarrier imaging plates. Cells were treated with 100 ng ml^{-1} of EGF-biotin/streptavidin-Alexa-647 complex, Invitrogen, E35351, equivalent to ~10 ng ml^{-1} of EGF for 30 min. Each condition (EGF stimulation time, treatment and mutation) was repeated in at least six wells. Eleven images (276 × 234 µm^2) were collected from each well by automated confocal microscope CV7000 (Yokogawa) with a ×60 water immersion objective (1.2 numerical aperture), with a total of 1,063 ± 251 (mean ± s.d.) imaged cells per well. Images were analyzed by MotionTracking software (http://motiontracking.mpi-cbg.de)[34,35] and 147 ± 80 (mean ± s.d.) EEA1-positive endosomes per cell were found. All statistics were calculated per image, then averaged between images in the well and, finally, averaged between wells of equal conditions. The s.e.m. was calculated from the last averaging step.

Generation of adherent HEK293 cells. Flp-In 293 TREx cells (Thermo Fisher) were grown at 37 °C/5% CO_2 in DMEM/10% FBS/1% PS media in six-well TC-treated plates to ~50–60% confluency. Cells were then transfected with pcDNA3.1 plasmid, expressing the gene for human Macrophage Scavenger Receptor 1 (*MSR1*) transcript variant A alongside G418 resistance cassette, using PolyJet transfection reagent (SignaGen), as per the manufacturer's instructions. Cells were grown overnight and then split into 10 cm plate containing 10 ml of DMEM/10% FBS/1% PS/800 µg ml^{-1} G418 and grown at 37 °C/5% CO_2 until distinct foci appeared. Individual foci were expanded, and screened for enhanced adherence using methylene blue staining and stringent washing in a 96-well plate format as previously described[10]. The most highly adherent cell line displaying robust growth in media and appropriate Flp-In 293 TREx resistance to Zeocin and Blasticidin was selected for use in the generation of MaMTH reporter cells.

Generation of stable MaMTH reporter cells. Reporter vector was generated in a pcDNA3.1(−) backbone using open reading frames (ORFs) expressing *G. princeps* luciferase (New England Biolabs) under the control of a 5xGAL4 UAS and puromycin resistance marker under the control of a constitutive PGK promoter, via Gibson assembly[36]. Adherent FLP-compatible HEK293 cells (prepared above) were grown at 37 °C/5% CO_2 in DMEM/10% FBS/1% PS media in six-well TC-treated plates to ~50–60% confluency. Cells were transfected with 1,000 ng reporter vector using X-tremeGENE 9 DNA transfection reagent (Roche) as per the manufacturer's instructions. After 5 h, media containing transfection reagent was removed and replaced with fresh DMEM/10%FBS/1%PS. Cells were grown for 48 h and then split one in two into new six-well plates using DMEM/10% FBS/1% PS + 0.5 µg ml^{-1} puromycin and grown until individual foci appeared. Individual foci were expanded, and monoclonal populations isolated by sorting of individual cells into 96-well plates using a fluorescence activated cell sorting Aria II Flow Cytometer (BD Biosciences), followed by further expansion. Expanded cell populations were screened individually and a cell line displaying strong MaMTH-responsive reporter activity and minimal background was selected for further use in MaMTH-DS.

Generation of Flp-In TREx compatible MaMTH bait vectors. Gateway cloning cassette followed by Cub-GAL4/RelA TF sequence was PCR-amplified from our previously reported MaMTH bait vector[4] using KAPA 2X HiFi DNA Polymerase (Kapa Biosystems). The amplified fragment was combined with EcoRV-digested Flp-compatible pcDNA5/FRT/TO vector (Thermo Fisher) via Gibson Assembly[36]. Generated constructs were fully sequence verified, and construct containing all of the elements necessary for Gateway cloning, tetracycline-induction, MaMTH bait C-tagging and use in generation of isogenic stables via the Flp-In TREx system, was isolated. This final bait vector construct was designated A1160 (Supplementary Note 1).

Generation of Flp-In TREx compatible MaMTH bait constructs. All bait and prey constructs were generated using the Gateway cloning technology (Thermo Fisher) and destination vectors A1160 (MaMTH bait) or A1245 (MaMTH prey, Supplementary Note 1). ShcI ORF in entry clone format was obtained from the Human ORFeome Collection v.8.1 (ref. [37]). EGFR-WT and single L858R and double L858R/T790M mutant entry clones were generated as described previously[4]. EGFR triple mutant containing the C797S mutation was generated via site-directed mutagenesis of EGFR double mutant using primers 5′-atgcccttcggcagcctcctggact-3′ and 5′- agtccaggaggctgccgaagggcat-3′. MET entry clone was obtained from OpenFreezer (V9936). All final bait and prey constructs were fully sequence verified.

Generation of double stable MaMTH bait cell lines. Isogenic MaMTH reporter cell lines stably expressing baits of interest were generated using the Flp-In TREx system (Thermo Fisher). Briefly, MaMTH reporter cells were grown at 37 °C/5% CO_2 in DMEM/10% FBS/1% PS media in six-well TC-treated plates to ~50–60% confluency. Cells were transfected with 900 ng pOG44 and 100 ng of bait construct in A1160 using X-tremeGENE 9 DNA transfection reagent (Roche) as per the manufacturer's instructions. After 5 h, media containing transfection reagent was removed and replaced with fresh DMEM/10% FBS/1% PS. Cells were grown for 48 h and then split one in two into new six-well plates using DMEM/10% FBS/1% PS + 100 µg ml^{-1} hygromycin and grown until individual foci appeared. Foci were expanded and proper, tetracycline-induced bait expression was verified by western blotting.

MaMTH-DS high-throughput screening workflow. MaMTH reporter cells stably expressing EGFR L858R/T790M/C797S bait or EGFR L858R/T790M control bait were seeded into 384-well plates (5,000 cells per well) in DMEM/10% FBS/1% PS media using a MultiDrop Combi (Thermo) fitted with a standard cassette. Plates were covered with MicroClime Environmental Lids (Labcyte, hydrated with ~10 ml ddH_2O) and grown at 37 °C/5% CO_2 overnight. The next day cells were transfected with 25 ng of MaMTH ShcI prey DNA using X-tremeGENE 9 DNA transfection reagent (Roche) as per the manufacturer's instructions. Transfection mix (5 µl total volume per well) was added to 384-well plates containing cells using a Bravo Automated Liquid Handling Platform (Agilent) fitted with a 96ST pipette head. Plates were once again covered with MicroClime Lids and grown at 37 °C/5% CO_2 for 5 h. Media was then removed from plates using a BioTek 405 Select microplate washer, and a fresh 50 µl of DMEM/10% FBS/1% PS media containing 0.5 µg ml^{-1} Tetracycline was added to each well using a MultiDrop Combi. Then, 50 nl of DMSO, osimertinib (70 µM) or library compound (10 mM for ChemBridge/Maybridge compounds, 1 mM for OICR TKIs) were added to individual wells using an ECHO 550 (Labcyte). Plates were covered with MicroClime Lids and grown for an additional 17–18 h at 37 °C/5% CO_2. Cells were then subjected to luciferase assay using 20 µl of 20 µM coelenterazine per well. Luminescence was measured in an injector-equipped SynergyNeo microplate reader, using linear shaking for 2 s after substrate addition. All reads were performed from the top using a Gain of 100 and a 1 s integration time.

Data analysis of MaMTH-DS screening results. All data analysis was performed in an automated fashion using in house-software developed in the R programming language[38]. Raw data from screens were subjected to Box–Cox transformation as previously described[39] to improve data distribution symmetry and normality. *Z* values were calculated on a per plate basis using EGFR L858R/T790M and EGFR L858R/T790M/C797S in the presence of osimertinib as positive and negative controls, respectively (with the exception of ShcI Round 2 Plate 10, where, due to a technical issue, EGFR L858R/T790M/C797S in the presence of DMSO was used as a negative control instead). Before *Z* calculations, the single most extreme value from each control dataset was excluded if it was classified as an outlier based on a cut-off of 1.5 times the interquartile range. Data normalization was performed using both controls-based NPI and sample-based (controls independent) B Score. NPI was calculated as (negative control signal – sample signal)/(negative control signal – positive control signal) × 100. B Score was calculated using the cellHTS2 package[40]. NPI was plotted against BScore and hits were scored using a combined cut-off of 70% NPI and a BScore of −3 or lower.

In vitro kinase assays. Kinase assays were performed using recombinant proteins of the kinase domain of wild-type EGFR, EGFR-C797S/T790M/L858R, EGFR-C797S/T790M/ex19del and EGFR-C797S (Reaction Biology Corporation). Compounds (Midostaurin, AZD7762, ChemBridge 5213777 and cilteritinib) were tested in a ten-dose IC_{50} duplicate mode with three-fold serial dilution starting at 10 µM. Reactions were carried out at 10 µM ATP.

Caspase 3 and 7 assays. PC9-C797S, A549 or HBE cells were seeded into 384-well plates at 5,000 cells per well. After 72 h of drug treatment, caspase 3 and 7 activity were measured using the Caspase-Glo 3/7 assay (Promega).

PC9 EGFR ex19del/T790M/C797S organoid viability assays. PC9 EGFR ex19del/T790M/C797s cells were adapted to grow in Matrigel conditions, to generate organoid cultures. In viability assays, organoids were dissociated to single cells and seeded on top of a thin layer of Matrigel in culture medium. Drugs were added after 3 d of culturing and grown in the absence or presence of drug for the indicated time period. Organoid viability was determined by ATP quantification using the CellTiter-Glo 3D luminescence-based assay (Promega). Organoid generation and screening were performed in Princess Margaret Living Biobank Facility (https://www.livingbiobank.ca/).

Surface biotinylation assays. HEK293 EGFR L858R/T790M/C797S cells were seeded at density of 200,000 cells per well in a six-well plate. Cells were serum-starved for 18 h and then treated with 10 µM compound for 2 h at 37 °C. Cells were then washed three times with ice-cold PBS and biotinylated using 2 mg ml^{-1} biotin for 30 min at 4 °C. Cells were washed three times with 100 mM glycine and lysed in lysis buffer (cell lysis buffer 10×, Cell Signalling Technology, no. 9803) supplemented with protease inhibitors. Lysates were transferred to 1.5 ml microtubes, and centrifuged for 16,000*g* for 10 min. Supernatants were transferred to fresh tubes, with 20% of the supernatant being kept as an input control. The remainder of the supernatant was used for pull-down using streptavidin beads. Pull-down of the beads and supernatants was carried out overnight at 4 °C on a rotating shaker. Beads were washed, resuspended in Laemmli sample buffer and heated at 95 °C for 5 min. Samples were run on a 12% SDS–PAGE gel and western blotting was performed.

EMI1 medicinal chemistry. EMI1 was purchased from InterBioScreen Ltd, with a purity greater than 95%. EMI7 was purchased from Life Chemicals Inc., with a purity greater than 99%. EMI1 medicinal chemistry synthesis schemes along with corresponding mass spectrometry, nuclear magnetic resonance and high-performance liquid chromatography data for each compound is provided in Supplementary Note 2.

Tracking of EB3-positive microtubule plus ends in cells. MaMTH reporter HEK293 cells stably expressing EGFR-WT or EGFR L858R/T790M/C797S were transfected with EB3-TagRFP. Cell were stimulated with 0.5 µg ml^{-1} tetracycline to induce EGFR expression 18 h before imaging. Cells were incubated with EMI for 30 min before imaging. Inverted research microscope Nikon Eclipse Ti-E (Nikon) supplemented with the perfect focus system (Nikon) and equipped with Nikon CFI Apo TIRF ×100 1.49 numerical aperture oil objective (Nikon), Photometrics Evolve 512 EMCCD (Roper Scientific) controlled with MetaMorph 7.7 software (Molecular Devices) was used to perform the live-cell imaging. Images were acquired in a stream mode with an exposure time of 500 ms. Kymographs were generated using ImageJ plugin KymoResliceWide (https://github.com/ekatrukha/KymoResliceWide). Parameters of microtubule dynamics were analyzed as described previously[41,42].

Microtubule imaging. PC9 EGFR ex19del/T790M/C797S cells were incubated with 1 µM of EMI1 for 20 h. Cells were fixed and immunostained for tubulin (1°, rat-anti-α-tubulin (YL1/2) (MA1-80017, Pierce Antibodies) antibody and 2°, Alexa-568 conjugated goat antibodies against rat IgG (Molecular Probes)). Nucleus was stained using DAPI. Imaging was performed with a Nikon Eclipse 80i upright fluorescence microscope equipped with Plan Apo VC 1.40 numerical aperture, oil ×100.

In vitro microtubule polymerization assays. To monitor the direct effects of EMI1 on microtubule dynamics, in vitro assays were performed as described previously using purified pig brain tubulin and mCherry-EB3 (ref. [43]).

Reporting Summary. Further information on research design is available in the Nature Research Reporting Summary linked to this article.

Data availability

All data supporting the findings presented in this study are available in the paper and its Supplementary Information files.

Code availability

All R code used in the analysis of the presented drug screening data is available from the authors on request.

References

34. Collinet, C. et al. Systems survey of endocytosis by multiparametric image analysis. *Nature* **464**, 243–249 (2010).
35. Rink, J., Ghigo, E., Kalaidzidis, Y. & Zerial, M. Rab conversion as a mechanism of progression from early to late endosomes. *Cell* **122**, 735–749 (2005).
36. Gibson, D. G. et al. Enzymatic assembly of DNA molecules up to several hundred kilobases. *Nat. Methods* **6**, 343–345 (2009).
37. Yang, X. et al. A public genome-scale lentiviral expression library of human ORFs. *Nat. Methods* **8**, 659–661 (2011).
38. R: a language and environment for statistical computing (R Core Team, 2017).
39. Box, G. E. P. & Cox, D. R. An analysis of transformations. *R. Stat. Soc.* **26**, 211–252 (1964).
40. Boutros, M., Brás, L. P. & Huber, W. Analysis of cell-based RNAi screens. *Genome Biol.* **7**, R66 (2006).
41. Aher, A. et al. CLASP suppresses microtubule catastrophes through a single TOG domain. *Dev. Cell* **46**, 40–58.e8 (2018).
42. Mohan, R. et al. End-binding proteins sensitize microtubules to the action of microtubule-targeting agents. *Proc. Natl Acad. Sci. USA* **110**, 8900–8905 (2013).
43. Jost, M. et al. Combined CRISPRi/a-based chemical genetic screens reveal that rigosertib is a microtubule-destabilizing agent. *Mol. Cell* **68**, 210–223 (2017).

Acknowledgements

We thank L. Riley for valuable discussions and editing of this manuscript. We also thank P.A. Jänne and M.J. Eck (both at Dana Farber Cancer Institute, Harvard Medical School, Boston, MA, USA) for providing us with the PC9-T790M and PC9-C797S cells used in our study, and the Center for Information Services and High Performance Computing of the TU Dresden for providing support and computational resources. This research was supported by funding from Consortium Québécois sur la Découverte du Médicament (CQDM) (Explore) and OCE (no. 23929). In addition, work in the Stagljar laboratory is supported by the Canadian Cancer Society Research Institute (no. 703889), Genome Canada via Ontario Genomics (grant nos, 9427 and 9428), Ontario Research fund (grant nos. ORF/DIG-501411 and RE08-009), CQDM (Quantum Leap) and Brain Canada (Quantum Leap, and Cancer Research Society (grant no. 23235)). J.H.P.'s work in the laboratory of Mark Lemmon at Yale was supported by National Institutes of Health grant nos. R01-CA198164 and R35-GM122485. G.P. acknowledges the support of the Ontario Institute for Cancer Research and its funding from the Government of Ontario.

Author contributions

P.S. performed preliminary MaMTH testing and validation/functional analysis of identified compounds, managed the project and wrote the manuscript. J.S. generated MaMTH reporter constructs and cells lines, performed MaMTH-DS screening and data analysis, managed the project and wrote the manuscript. Y.K. and M.Z. performed and analyzed the high-throughput EGFR microscopy data. K.W., L.D., A.L., N.V., A.V., S.P., F.A., Z.Y. and V.W. performed construct generation, preliminary MaMTH validation and were involved in the validation/functional analysis of compounds. N.R., N.A.P., Y.W., A.S. and M.S.T. generated and validated organoids and provided cell lines. A.R. and A.A. performed and analyzed microtubule dynamics data. L.E.W.G., A.D. and J.W. performed MaMTH-DS screening. B.T., A.A., M.P., B.J., R.M., D.U. and R.A. performed medicinal chemistry and assisted technically throughout the whole project. G.P. performed computational chemistry, molecular docking and hit expansion. J.H.P. assisted with computational modeling and undertook some biochemical studies. R.M.S., M.J., M.S., M.F.M., N.L. and F.A.S. provided clinical expertise and support. All authors discussed the results and commented on the manuscript. I.S. initiated and supervised the project and wrote the manuscript.

Competing interests

I.S., P.S. and J.S. (in conjunction with the University of Toronto) are listed as inventors on a patent (publication no. 20190091205) for the use of EMI1 (and structurally related analogs), midostaurin, gilteritinib and AZD7762 (and structurally related analogs) in the treatment of mutant EGFR-mediated NSCLC.

Additional information

Supplementary information is available for this paper at https://doi.org/10.1038/s41589-020-0484-2.

Correspondence and requests for materials should be addressed to I.S.

Reprints and permissions information is available at www.nature.com/reprints.

nature research

Corresponding author(s): Igor Stagljar

Last updated by author(s): Dec 30, 2019

Reporting Summary

Nature Research wishes to improve the reproducibility of the work that we publish. This form provides structure for consistency and transparency in reporting. For further information on Nature Research policies, see Authors & Referees and the Editorial Policy Checklist.

Statistics

For all statistical analyses, confirm that the following items are present in the figure legend, table legend, main text, or Methods section.

n/a	Confirmed
☐	☒ The exact sample size (*n*) for each experimental group/condition, given as a discrete number and unit of measurement
☐	☒ A statement on whether measurements were taken from distinct samples or whether the same sample was measured repeatedly
☐	☒ The statistical test(s) used AND whether they are one- or two-sided *Only common tests should be described solely by name; describe more complex techniques in the Methods section.*
☒	☐ A description of all covariates tested
☐	☒ A description of any assumptions or corrections, such as tests of normality and adjustment for multiple comparisons
☐	☒ A full description of the statistical parameters including central tendency (e.g. means) or other basic estimates (e.g. regression coefficient) AND variation (e.g. standard deviation) or associated estimates of uncertainty (e.g. confidence intervals)
☐	☒ For null hypothesis testing, the test statistic (e.g. *F*, *t*, *r*) with confidence intervals, effect sizes, degrees of freedom and *P* value noted *Give P values as exact values whenever suitable.*
☒	☐ For Bayesian analysis, information on the choice of priors and Markov chain Monte Carlo settings
☒	☐ For hierarchical and complex designs, identification of the appropriate level for tests and full reporting of outcomes
☒	☐ Estimates of effect sizes (e.g. Cohen's *d*, Pearson's *r*), indicating how they were calculated

Our web collection on statistics for biologists contains articles on many of the points above.

Software and code

Policy information about availability of computer code

Data collection	EGFR localization and trafficking assay images were analyzed by MotionTracking software (http://motiontracking.mpi-cbg.de). This software is used and described in the following cited papers: Collinet, C. et al. Systems survey of endocytosis by multiparametric image analysis. Nature 464, 243–9 (2010). Rink, J., Ghigo, E., Kalaidzidis, Y. & Zerial, M. Rab conversion as a mechanism of progression from early to late endosomes. Cell 122, 735–749 (2005). MetaMorph 7.7 software (Molecular Devices) was used to perform the live cell imaging.
Data analysis	EGFR localization and trafficking assay images were analyzed by MotionTracking software (http://motiontracking.mpi-cbg.de). This software is used and described in the following cited papers: Collinet, C. et al. Systems survey of endocytosis by multiparametric image analysis. Nature 464, 243–9 (2010). Rink, J., Ghigo, E., Kalaidzidis, Y. & Zerial, M. Rab conversion as a mechanism of progression from early to late endosomes. Cell 122, 735–749 (2005). Kymographs were generated using ImageJ plugin KymoResliceWide (https://github.com/ekatrukha/KymoResliceWide). GraphPad v8.3.0 was used to generate graphs and data analysis.

For manuscripts utilizing custom algorithms or software that are central to the research but not yet described in published literature, software must be made available to editors/reviewers. We strongly encourage code deposition in a community repository (e.g. GitHub). See the Nature Research guidelines for submitting code & software for further information.

Data

Policy information about availability of data

All manuscripts must include a data availability statement. This statement should provide the following information, where applicable:

- Accession codes, unique identifiers, or web links for publicly available datasets
- A list of figures that have associated raw data
- A description of any restrictions on data availability

All data supporting the findings presented in this study are available within the paper and its supplementary information files.

Field-specific reporting

Please select the one below that is the best fit for your research. If you are not sure, read the appropriate sections before making your selection.

☒ Life sciences ☐ Behavioural & social sciences ☐ Ecological, evolutionary & environmental sciences

For a reference copy of the document with all sections, see nature.com/documents/nr-reporting-summary-flat.pdf

Life sciences study design

All studies must disclose on these points even when the disclosure is negative.

Sample size	All experiments were performed with a minimum sample number of 3 biological replicates, unless stated otherwise. For the dose-response experiments assessing the EC50 on organoid viability, individual 36 point dose-response curves were generated. Sample sizes were chosen based on previous experience for each experiment. No statistical methods were used to predetermine sample size.
Data exclusions	No data was excluded
Replication	The exact numbers of replications are noted in the figure legends. The key experiments were replicated for 2-3 times and all attempts were successful. Key experiments, including western blots, viability assays, caspase assays and MaMTH assays were replicated by multiple investigators.
Randomization	No animal or human subjects were used for this study, so the need for randomization was not necessary
Blinding	Binding was not conducted for this study, as all data was quantitative in nature, with no qualitative data assessed.

Reporting for specific materials, systems and methods

We require information from authors about some types of materials, experimental systems and methods used in many studies. Here, indicate whether each material, system or method listed is relevant to your study. If you are not sure if a list item applies to your research, read the appropriate section before selecting a response.

Materials & experimental systems

n/a	Involved in the study
☐	☒ Antibodies
☐	☒ Eukaryotic cell lines
☒	☐ Palaeontology
☒	☐ Animals and other organisms
☒	☐ Human research participants
☒	☐ Clinical data

Methods

n/a	Involved in the study
☒	☐ ChIP-seq
☒	☐ Flow cytometry
☒	☐ MRI-based neuroimaging

Antibodies

Antibodies used	All the antibodies used in the study, including information on where they are from, dilutions and catalog numbers are provided in the materials and methods sections. Briefly, the following antibodies were used: phospho-EGFR antibody (Tyr1173; Santa Cruz, sc101668, 1:10,000) total EGFR (Cell Signalling Technology, #4267, 1:10,000) phospho-AKT (Ser473; Cell Signalling Technology, #4060, 1:10,000) total AKT (Cell Signalling Technology, #4691, 1:10,000) phospho-ERK1/2 (Thr202/Tyr204; Cell Signalling Technology, #9101, 1:10,000) total ERK1/2 (Cell Signalling Technology, #9102, 1:10,000) phospho S6 (Ser240/244; Cell Signalling Technology, #5364, 1:10,000) total S6 (Cell Signalling Technology, #5364, 1:10,000) total GAPDH (Santa Cruz, 1:10,000)

total tubulin (SantaCruz, 1:10,000)
anti-V5 (Cell Signalling Technology, 1:10,000)

Validation

All the antibodies used in this study were commercially available and tested/validated in multiple publications. Detailed descriptions for each antibody including quality control can be found on the respective manufacturers product sheet.

Eukaryotic cell lines

Policy information about cell lines

Cell line source(s)

The following cell lines were purchased from ATCC: HEK293, A549, HBE.

PC9 cells were provided by P.A. Jänne and M.J. Eck.

Authentication

All cell were initially authenticated using STR analysis at the Sick Kids authentication facility.

Mycoplasma contamination

All cell lines were initially tested and confirmed to be negative for mycoplasma contamination.

Commonly misidentified lines
(See ICLAC register)

No cell lines used are listed in the database of commonly misidentified cell lines.